# Ligand-Induced Heme Ruffling and Bent NO Geometry in Ultra-High-Resolution Structures of Nitrophorin 4[†,‡]

Sue A. Roberts,[§] Andrzej Weichsel,[§] Yan Qiu,[||] John A. Shelnutt,[||] F. Ann Walker,[§] and William R. Montfort*[,§]

*Departments of Biochemistry and Molecular Biophysics, and Chemistry, University of Arizona, Tucson, Arizona 85721, Biomolecular Materials and Interfaces Department, Sandia National Laboratories, Albuquerque, New Mexico 87185-1349, and Department of Chemistry, University of New Mexico, Albuquerque, New Mexico 87131*

*Received May 7, 2001; Revised Manuscript Received August 6, 2001*

ABSTRACT: The nitrophorins are a family of proteins that use ferric heme to transport nitric oxide (NO) from the salivary glands of blood-sucking insects to their victims, resulting in vasodilation and reduced blood coagulation. We have refined atomic resolution structures of nitrophorin 4 (NP4) from *Rhodnius prolixus* complexed with NO (1.08 Å) and $NH_3$ (1.15 Å), yielding a highly detailed picture of the iron coordination sphere. In NP4−NO, the NO nitrogen is coordinated to iron (Fe−N distance = 1.66 Å) and is somewhat bent (Fe−N−O angle = 156°), with bending occurring in the same plane as the proximal histidine ring. The Fe(NO)(heme)(His) coordination geometry is unusual but consistent with an Fe(III) oxidation state that is stabilized by a highly ruffled heme. Heme ruffling occurs in both structures, apparently due to close contacts between the heme and leucines 123 and 133, but increases on binding NO even though the steric contacts have not changed. We also report the structure of NP4 in complexes with histamine (1.50 Å) and imidazole (1.27 Å). Unexpectedly, two mobile loops that rearrange to pack against the bound NO in NP4−NO, also rearrange in the NP4−imidazole complex. This conformational change is apparently driven by the nonpolar nature of the NO and imidazole (as bound) ligands. Taken together, the desolvation of the NO binding pocket through a change in protein conformation, and the bending of the NO moiety, possibly through protein-assisted heme ruffling, may lead to a nitrosyl−heme complex that is unusually resistant to autoreduction.

Nitric oxide (NO),[1] a ubiquitous signaling molecule in vertebrates, is synthesized by NO synthase and detected by soluble guanylate cyclase, two heme proteins (recently reviewed in refs *1*−*4*). This creates a challenge for Nature in that NO is reactive toward heme iron and the oxidation state of the heme in these proteins must therefore be carefully regulated. For example, soluble guanylate cyclase uses ferrous [Fe(II)] heme to tightly bind NO (binding affinity ≈ $10^{12}$ $M^{-1}$), which stimulates cyclase activity, but then must somehow release NO in order to turn off the cyclase signal. NO synthase cycles between ferrous and ferric forms while functioning, and apparently suffers from product inhibition by NO. The nitrophorins from *Rhodnius prolixus* (*5*) and *Cimex lectularius* (*6*) require a ferric heme (binding affinity ≈ $10^6$ $M^{-1}$) for storing NO in the salivary gland in a form that can be readily released during feeding.

Heme-containing proteins are numerous and participate in a large variety of reactions, including electron transfer (e.g., cytochrome *c*), transport of gaseous molecules (e.g., hemoglobin), and catalysis (e.g., cytochrome P450). To perform these diverse functions, heme-containing proteins must stabilize appropriate iron oxidation states, provide a range of oxidation potentials for the iron-heme center, and discriminate between ligands. It is clear that the heme rings in proteins are often distorted from planarity and that the type of distortion seen often correlates with protein function (*7*). Distortions of the heme ring can be caused by protein imposed steric crowding or through covalent linkages between the protein residues and the heme. As the heme ring deviates from planarity, the electronic and chemical properties of the heme iron are altered. Despite these general conclusions, the role of heme distortion in the setting of heme properties is not well characterized, in part due to the sparseness of atomic resolution structures for heme proteins.

Nitrophorin 4 (NP4) is one of four NO transport proteins from the saliva of the bloodsucking insect *Rhodnius prolixus* (recently reviewed in refs *8* and *9*). The *Rhodnius* nitrophorins transport NO from the salivary glands of the insects to the tissue of a potential victim, where it is released and induces vasodilation. The proteins also bind tightly to histamine, which is released by the victim in response to the tissue damage caused by the feeding insect. Crystal structures have been determined for three of the four *Rhodnius* nitrophorins, and all have a lipocalin fold, consist-

[†] This work was supported in part by National Institutes of Health grants HL62969 to W.R.M and HL54826 to F.A.W.

[‡] Coordinates for the NP4−NO, NP4−$NH_3$, NP4−histamine, and NP4−imidazole complexes have been deposited with the Protein Data Bank (PDB entries 1IKH, 1D2U, 1IKE, 1IKJ).

* To whom correspondence should be addressed. E-mail: montfort@email.arizona.edu.

[§] University of Arizona.

[||] Sandia National Laboratories and University of New Mexico.

[1] Abbreviations: NP1−4, *Rhodnius prolixus* nitrophorins 1−4; NO, nitric oxide; Fe(II), ferrous iron; Fe(III), ferric iron; $K_d^{III}$, dissociation constant for ligand from ferric nitrophorin; $K_d^{II}$, dissociation constant for ligand from ferrous nitrophorin; OEP, octaethylporphyrinato dianion.

10.1021/bi0109257 CCC: $20.00 
Published on Web 08/28/2001

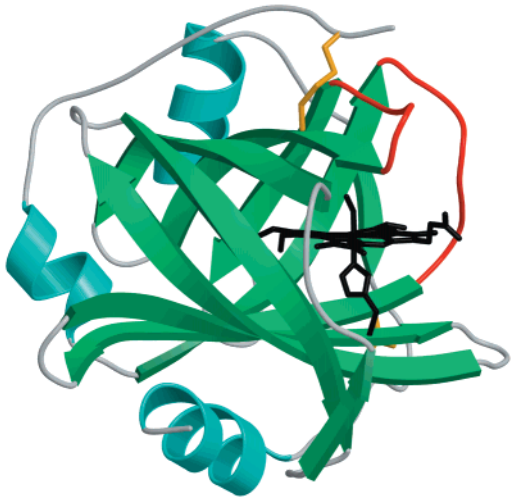

FIGURE 1: Ribbon drawing of NP4−NO. Heme, His 59, and NO are shown in black, disulfide bonds in yellow, and mobile loops A−B (residues 31−37, connecting $\beta$-strands A and B, right edge), and G−H (residues 125−132), which collapse around NO upon NO ligation, are shown in red.

ing of a $\beta$-barrel with heme inserted into one end of the barrel and attached to the protein through a proximal histidine (refs *10*−*12*; Figure 1). All the nitrophorins have highly nonplanar, ruffled hemes. Ligands bind to the distal side of the heme, which is part of a large, open cavity when the axial ligand is cyanide, histamine, ammonia, or water. It was demonstrated with NP4, however, that NO binding causes two flexible loops to pack around the NO (Figure 1), forming a hydrophobic pocket and stabilizing the ferric NO complex (*13*). The proteins display biphasic NO binding and release kinetics that are most likely related to the rates by which these loops move in to and out of the distal pocket (*14*). Release is approximately 10-fold faster at pH 8 than at pH 5, consistent with the protein's function to release NO into the victim's tissue (pH ~7.4) but to store NO in the insect's salivary gland (pH ~5).

The nitrophorins require a ferric heme to function as NO transport and histamine binding proteins. In NP4, reduction of iron to Fe(II) causes nearly irreversible binding of NO ($K_d^{III}/K_d^{II} \approx 10^6$), and, furthermore, leads to weaker histamine binding ($K_d^{III}/K_d^{II} = 8 \times 10^{-3}$) (*14*, *15*). The heme reduction potentials are about 300 mV more negative for the nitrophorins than for metmyoglobin, which requires ferrous heme to function in oxygen storage (*14*, *15*). This corresponds to a stabilization of the nitrophorin ferric heme by about 7 kcal mol$^{-1}$ with respect to the same heme placed in the globin protein fold. The mechanism by which the nitrophorins stabilize the ferric state is not yet clear, but may be due in part to heme ruffling.

In this paper, we report the extension to atomic resolution of two known NP4 structures, NP4−NO and NP4−$NH_3$. In these structures, now at 1.08 and 1.15 Å resolutions, respectively, we have been able to refine the conformation of the iron coordination sphere and heme ring without geometrical restraints, providing a clear view of the highly ruffled nitrophorin heme in the presence and absence of NO, and demonstrating that NO binding leads to an increase in heme ruffling. The NO geometry is also clarified in the present work. The previous structure of NP4−NO, determined to 1.4 Å resolution using 1.54 Å X-rays, was complicated by a disorder at the NO position that was fit with two Fe−NO coordination geometries, one containing a nearly linear Fe−N−O bond and the other a nearly side-on bond. The present structure, determined with 0.98 Å X-rays, displays a single NO geometry that is somewhat bent. We also report the structure of NP4−histamine at 1.5 Å and NP4−imidazole at 1.27 Å. These four structures, in comparison with those reported previously (*13*), allow us to specify the factors contributing to the ruffling of the heme in NP4, discuss the bonding in the Fe(NO)(heme) complex relative to that of Fe(NO)porphyrin complexes and to appreciate how the Fe(III)NO complex is stabilized over Fe(II)NO in this protein.

## MATERIALS AND METHODS

NP4 was overexpressed in *Escherichia coli*, isolated from inclusion bodies, renatured and crystallized as previously described (*11*, *13*, *16*). Crystals were grown under two conditions, in 2.6 M ammonium phosphate (pH 7.5), and in 22% PEG 4000 (pH 5.6). Despite large changes in crystallization conditions, the crystals are isomorphous. For data measurement, crystals were picked up in a cryoloop (Hampton) and flash-frozen in liquid nitrogen or in a cooled nitrogen gas stream.

*NP4*−*$NH_3$ (pH 7.5).* Diffraction data were measured at the ESRF synchrotron (beam line BM1A of the SNBL), using a MAR imaging plate, and were reduced using DENZO (*17*), and CCP4 (*18*).

*NP4*−*NO.* A single NP4 crystal (pH 5.6) was equilibrated for 2 h in a solution at pH 5.6 containing 50% PEG 4000 and 100 mM sodium citrate, and saturated with argon, followed by 1 h equilibration in a similar solution saturated with NO. A 1.0 Å data set was measured on beam line X12B at the NSLS at Brookhaven National Laboratory with an ADSC Quantum-4 CCD detector. Data were processed with HKL (*17*).

*NP4-Histamine.* A crystal of NP4 (pH 5.6) was soaked for 20 h in a solution containing 10 mM histamine, 30% PEG 4000, buffered with citric acid at pH 5.6, then transferred to a similar solution containing 50% PEG 4000 before being frozen for data collection. The data were collected on a Nonius FAST/FR571 system using CuK$\alpha$ radiation. Data were processed with PROCOR (*19*) and SCALA (*18*).

*NP4-Imidazole.* Crystals were grown from a solution containing NP4 and 20 mM imidazole in 22% PEG 4000, 100 mM sodium citrate, at pH 5.6. The data were measured with a Rigaku RAXISIV++ using CuK$\alpha$ radiation from a Rigaku R3HR generator focused with Osmic mirrors. Data were processed using D*TREK (*20*).

For all structures, models were built using O (*21*), and refined with SHELXL (*22*). The final models for NP4−NO, NP4−$NH_3$, and NP4−imidazole were refined using the conjugate gradient approach of SHELXL, with anisotropic temperature factors, and no distance or van der Waals restraints on the heme iron. Hydrogen atoms were included at calculated positions and not refined. For heme coordination sphere error analysis (Table 2), several cycles of full-matrix refinement were performed with the iron coordination sphere (heme, His 59, and $NH_3$, NO, or imidazole) completely

Table 1: Crystallographic Data Measurement and Refinement Parameters for NP4 Complexes

| complex | NO | $NH_3$ | histamine | imidazole |
|---|---|---|---|---|
| PDB accession code | 1IKH | 1D2U | 1IKE | 1IKJ |
| space group | *C*2 | *C*2 | *C*2 | *C*2 |
| cell parameters | | | | |
| *a* | 70.15 | 69.92 | 70.18 | 70.18 |
| *b* | 42.42 | 42.69 | 42.60 | 42.48 |
| *c* | 52.94 | 52.75 | 52.80 | 52.96 |
| $\beta$ | 94.22 | 93.80 | 94.00 | 94.28 |
| pH/temp (K) | 5.6/100 | 7.5/100 | 5.6/140 | 5.6/100 |
| wavelength (Å) | 0.975 | 0.873 | 1.54 | 1.54 |
| resolution (Å) | 30−1.08 | 52−1.15 | 8.9−1.5 | 22−1.27 |
| total/unique reflections | 416 438/83 813[a] | 118 648/49 629 | 46 329/22 265 | 99 030/40 637 |
| completeness (%)[b] | 95/70 | 90/74 | 89/75 | 96/79 |
| mean $I/\sigma_I$[b] | 38./15. | 22.4/4.3 | 11.6/3.5 | 13.8/9.2 |
| $R_{sym}$[b] | 0.04/0.20 | 0.04/0.26 | 0.07/0.16 | 0.032/0.065 |
| $R_{cryst}/R_{free}$[c] | 0.12/0.15 | 0.13/0.19 | 0.18/0.24 | 0.13/0.17 |
| rmsd bonds/angles (Å) | 0.016/0.033 | 0.015/0.037 | 0.008/0.025 | 0.013/0.035 |
| disallowed $\varphi/\psi$ angles | 0 | 0 | 0 | 0 |
| data/parameter ratio[d] | 3.8 | 3.2 | 2.8 | 2.3 |
| no. of solvent atoms | 264 | 249 | 253 | 274 |
| no. of atoms disordered[e] | 26 | 14 | 15 | 62 |
| avg *B* (isotropic, Å$^2$) | | | | |
| overall protein | 13.0 | 15.9 | 19.9 | 10.6 |
| distal ligand | 11.9 | 10.8 | 17.1 | 8.5 |

[a] Includes data to 1.0 Å resolution; 62 762 unique reflections to 1.08 Å were used in refinement. [b] Overall/outer shell. [c] Crystallographic *R*-factor for working/test set (5% of reflections). [d] Values for the NO, $NH_3$, and imidazole complexes include anisotropic temperature factors. [e] Atoms discretely disordered and built in multiple conformations.

Table 2: Geometrical Parameters for NP4 Coordination Spheres

| distal ligand | resolution (Å) | distances, iron coordination sphere (Å)[a] | | | | | | planarity[b] (Å) | angle Fe-lig. (deg) |
|---|---|---|---|---|---|---|---|---|---|
| | | Fe−NA | Fe−NB | Fe−NC | Fe−ND | Fe−N$\epsilon$2 | Fe-lig | | |
| NO | 1.08 | 1.98 (1) | 1.99 (1) | 2.00 (1) | 2.00 (1) | 2.013 (9) | 1.66 (1) | 0.023 | 156 (1) |
| $NH_3$ | 1.15 | 1.99 (2) | 1.99 (2) | 2.00 (2) | 2.00 (2) | 1.97 (2) | 2.05 (2) | 0.023 | n/a |
| $CN^-$ | 1.60 | 1.94 | 1.95 | 2.05 | 1.89 | 1.96 | 1.93 | 0.009 | 158 |
| Hist. | 1.50 | 1.96 | 2.00 | 2.05 | 2.01 | 2.00 | 2.04 | 0.000 | n/a |
| $H_2O$ | 1.40 | 2.03 | 2.04 | 1.99 | 2.04 | 2.01 | 2.06 | 0.015 | n/a |
| Im | 1.27 | 1.98 (1) | 2.02 (1) | 2.00 (1) | 1.95 (1) | 1.95 (1) | 2.02 (1) | 0.038 | n/a |

[a] Numbers in parentheses are estimated standard deviations calculated after full-matrix refinement of the heme without restraints (see Materials and Methods). [b] Planarity is the RMS deviation of pyrrole nitrogen atoms from a least squares plane. For the ammonia, histamine, and aqua complexes, the heme iron lies in this plane (deviation $\sim$ 0.01 Å), while for the nitrosyl and cyano complexes, the heme iron lies slightly above this plane into the distal pocket ($\sim$0.06 Å).

unrestrained, and all other atoms fixed. For NP4−histamine, only Fe and S atoms were refined anisotropically. Hydrogen atoms were not included in the calculation and full-matrix refinement was not performed. Figures were produced using MOLSCRIPT (*23*), BOBSCRIPT (*24*), and RASTER3D (*25*).

Density functional theory (DFT) calculations were performed using DMOL (MSI, Inc., 9685 Scranton Road, San Diego, CA 92121−2777) on Fe(NO)(imidazole)(porphyrin) with all substituents removed from the porphyrin ring. The coordinate system had the NO and imidazole N atoms along the *z*-axis and the porphyrin nitrogen atoms along the *x*- and *y*-axes. Idealized symmetry was not imposed; the ruffling that exists in the crystal structure was present in the model. Spin-unrestricted VWN functionals were used with inner-core orbitals frozen. Vibrational and Mulliken analyses were performed using defaults in DMOL. Normal-coordinate Structural Decomposition calculations (NSD) were performed as described previously (*26*).

## RESULTS

*NP4−NO at 1.08 Å Resolution.* The complex NP4−NO, pH 5.6, was examined while frozen using synchrotron radiation, resulting in a structure at the ultra-high nominal resolution of 1.08 Å. The initial model was from a structure of the same complex measured in-house to 1.4 Å resolution (*13*), and as expected, there are no large differences between that structure and the one reported herein. The new data permitted the refinement of anisotropic temperature factors for the protein, the modeling of several residues in multiple conformations, including the heme and two disulfide-linked cysteines, inclusion of hydrogen atoms at calculated positions, and the unconstrained, full-matrix refinement of the entire iron coordination sphere, including the heme, NO, and proximal histidine residue. The unconstrained refinement allowed us to remove model bias from the iron coordination sphere, accurately estimate errors in atomic positions, and more reliably compare our model with related small-molecule structures. The final structure yields working and test *R*-factors of 0.12 and 0.15, respectively, demonstrating excellent correlation with the observed diffraction data (Table 1).

The most striking difference between the lower and higher resolution structures is the ordered NO ligand. In the previous work, the NO ligand occupied at least two orientations in the crystal (*13*). In the present structure, the electron density, shown in Figure 2, is consistent with a single NO conforma-

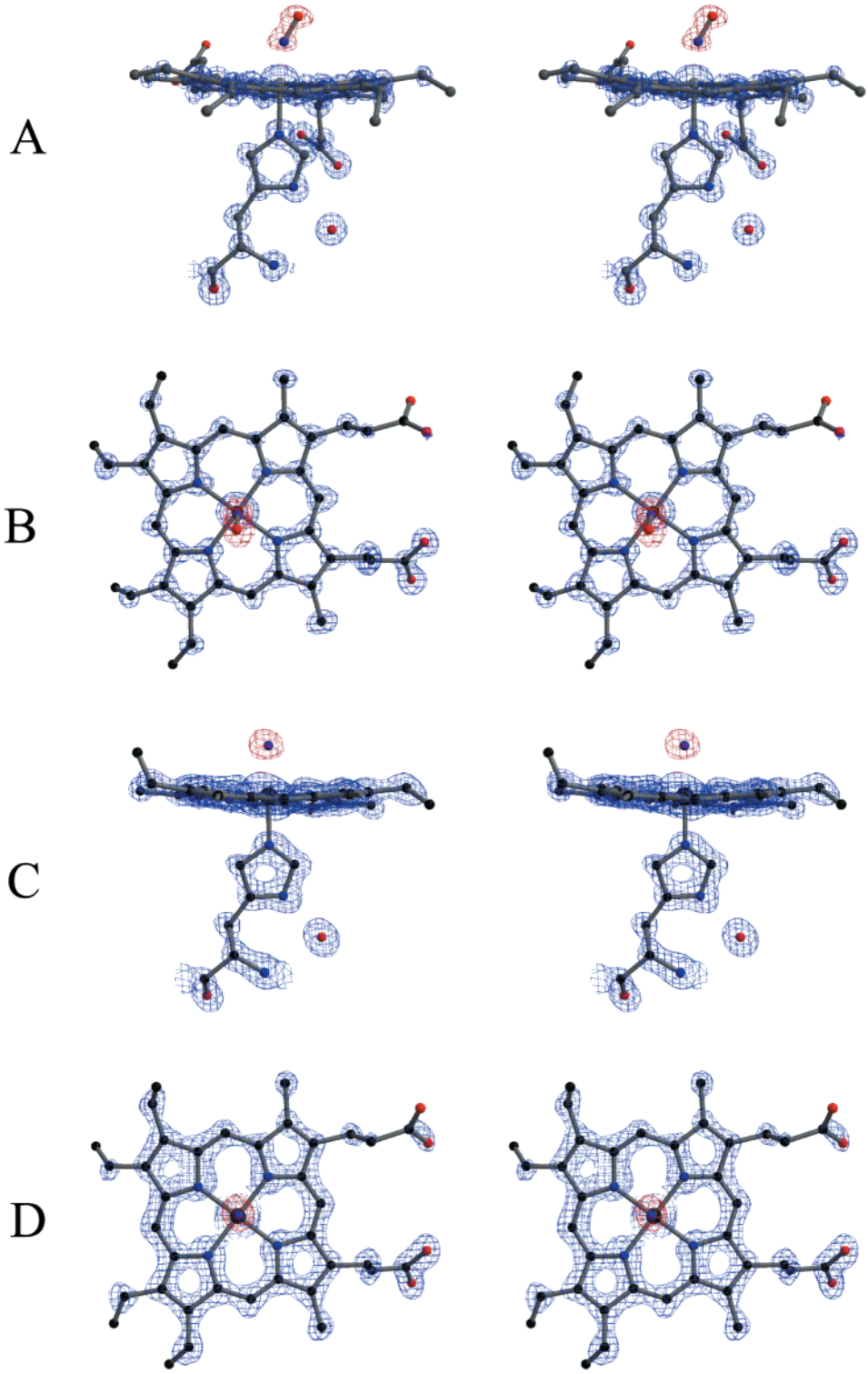


FIGURE 2: Electron density (coefficients are $2|F_o| - |F_c|$) for the coordination sphere. Shown are views from the edge and from the distal pocket for (a, b) NP4−NO (contoured at 2.5 $\sigma$), and (c, d) NP4−$NH_3$ (contoured at 2.5 $\sigma$). Because the heme resides in the pocket in two orientations that intermix the methyl and the vinyl substituents, the refined positions for two sets of half occupied vinyl C$\beta$ atoms are shown. The other heme atoms, including the proprionate substituents, occupy a single orientation. Pyrrole ring A is in the lower right-hand corner of the figure and rings B−D following in a clockwise fashion around the heme. The ligand electron density is shown in red for clarity.

tion with an Fe−N bond distance of 1.66 (1) Å and an Fe−N−O bond angle of 156 (2)° (numbers in parentheses are estimated standard deviations in the previous derived quantity). The Fe−N−O is bent such that all three atoms lie in the plane of His 59, the proximal trans ligand. This plane roughly bisects the heme through the atoms connecting pyrrole rings A and B (CHA), and pyrrole rings C and D (CHC; Figure 2). Figure 3 shows views of the Fe coordination sphere atoms contoured as 50% probability ellipsoids. As shown in the figure, the thermal ellipsoid for the NO oxygen, in contrast to the ellipsoids of Fe, its nitrogen ligands, and the atoms in the heme ring, is decidedly

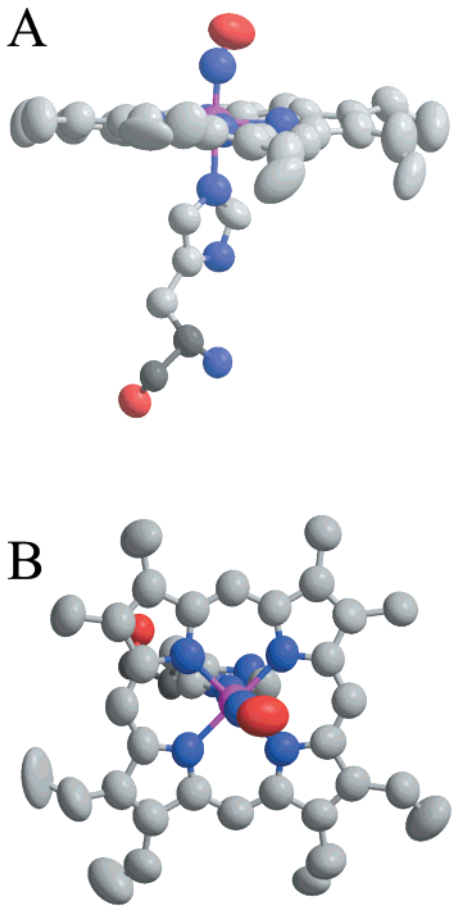


FIGURE 3: Anisotropic temperature factors for the iron coordination sphere in the NP4−NO complex. Atoms are contoured as 30% probability ellipsoids. Heme carboxylate groups have been removed for clarity. (a) Side view, emphasizing motion of the NO oxygen atom (in red). (b) View down the ON−Fe bond.

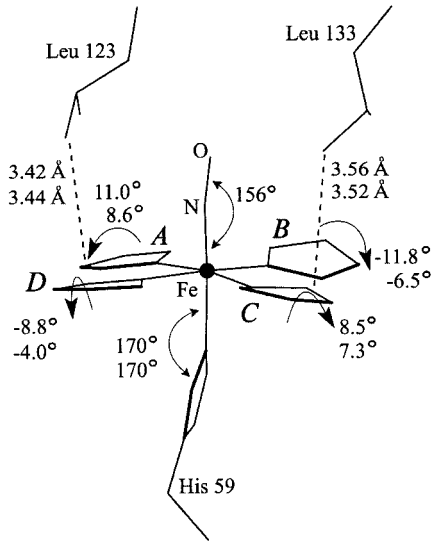


FIGURE 4: View of the heme coordination sphere for NP4−NO illustrating the pyrrole ring rotations that define the ruffling distortion. All non-pyrrole atoms are omitted for clarity. The extent of pyrrole rotation is indicated for NP4−NO (upper numbers) and NP4−$NH_3$ (lower numbers), as are the deviation of axial ligands from linear. Also shown are the two close contacts by leucine side chains that may contribute to the heme distortion.

Table 3: Heme Distortion from Planarity in NP4 Complexes

| ligand | $B_{1u}$[a] (ruffling) | $B_{2u}$[a] (saddling) | $\Phi_A$[b] | $\Phi_B$[b] | $\Phi_C$[b] | $\Phi_D$[b] | $\lvert\Phi\rvert$[b] |
|---|---|---|---|---|---|---|---|
| NO | −0.854 | 0.333 | 11.0 | -11.8 | 8.5 | −8.8 | 10.0 |
| $NH_3$ | −0.585 | 0.281 | 8.6 | −6.5 | 7.3 | −4.0 | 6.6 |
| CN | −0.816 | 0.393 | 11.6 | -10.6 | 10.2 | −6.0 | 9.6 |
| histamine | −0.524 | 0.242 | 9.4 | −5.9 | 4.6 | −6.6 | 6.6 |
| $H_2O$ | −0.528 | 0.246 | 8.0 | −7.0 | 8.9 | −4.6 | 7.1 |
| imidazole | −0.422 | 0.306 | 6.9 | −5.3 | 7.4 | −4.0 | 5.9 |

[a] Heme distortions in angstroms, as defined in ref *26*. [b] Rotation angle of pyrrole ring relative to the mean plane containing the nitrogen heme atoms. A positive rotation is defined as clockwise when looking down the nitrogen−iron bond, as illustrated in Figure 4.

nonspherical and elongated in the plane of the proximal histidine, indicating that the NO bond angle is easily deformable in this plane. Other bond distances and angles for the iron coordination sphere are listed in Table 2.

As noted previously (*13*), NO binding induces an extensive conformational change in the protein, resulting in the packing of two mobile protein loops against the bound NO. van der Waals contacts occur between NO and Leu 133 (C$\delta$2, 3.40 Å), Leu 130 (C$\delta$2, 3.83 Å), Wat 238 (3.72 Å), and Leu 123 (C$\beta$, 3.79 Å). If the Fe−N−O bond angle were linear, the first three of these distances would decrease, suggesting there could be a steric contribution to the bending of the Fe−N−O bond. However, the NP4 cyano complex (*13*) also displays a bent Fe−L bond without steric crowding by neighboring atoms, suggesting the cause of the bending may be electronic and that it may be correlated with heme ruffling. This possibility is further explored in the discussion section.

The nitrophorin heme is severely distorted from planarity, probably due in part to van der Waals contacts with Leu 123 and Leu 133 (Figure 4). Analysis of the heme conformation in terms of the lowest energy out-of-plane distortions, using the normal-coordinate structural decomposition (NSD) method developed by Shelnutt and co-workers (*7*), shows the distortion to be predominately "ruffling" ($B_{1u}$), characterized by a rotation of the pyrrole rings about the Fe−N bonds. Opposing rings rotate in the same sense, with, in this case, rings A and C rotating clockwise (as viewed along the N−Fe bonds from the pyrrole nitrogen to the heme iron), and rings B and D rotate counterclockwise (Figure 4). The difference in the ruffling for the 1.4 Å structure and the 1.08 Å structure is less than 1%. A minor "saddling" ($B_{2u}$) distortion also exists (Table 3), where two opposing pyrrole rings tip up, and two tip down, and the difference in saddling for the two structures is 7%. The NP4 ruffling, which is already the largest known for any noncovalently linked heme, increases substantially upon NO binding, with the average pyrrole rotation increasing from ∼7 to ∼10° (Table 3). The heme iron also shifts slightly on NO binding, moving 0.06 Å out of the plane of the pyrrole nitrogen atoms toward the NO ligand.

The higher resolution data allowed improved modeling of the inherent disorder in the protein. The heme is discretely disordered, by a 2-fold rotation about the CHA-CHC axis, as previously noted (*13*), with 50% of the heme refining as "right-side-up" and 50% as "upside-down". The only evidence of this disorder was weak electron density in omit maps at all four possible vinyl carbon positions. All other atoms, including the propionates, are superimposable with their counterparts in the alternate conformation, so it was only necessary to model alternate conformations for the vinyl atoms. This was accomplished by refining a model with a

single heme having four partially occupied vinyl carbons, as shown in Figure 2. Random heme insertion has been reported for other *b*-heme proteins, among them cytochrome $b_5$ (*27*−*29*), and is not expected to be of functional importance in NP4 since, for example, NP2 has only a single heme orientation (*12*) but displays kinetic behavior similar to NP4 (*14*). In addition to the heme disorder, residues 50, 81, 115, 119, and the disulfide-linked pair Cys 41−Cys 171 clearly occupy two conformations, and the Val 71 side chain occupies all three low-energy rotomers.

There are many second-shell water molecules clearly visible in the final electron density map, some of which bridge between symmetry related hydrated protein molecules. Greater than 95% of the unit cell volume is occupied by protein and ordered solvent atoms in the final model. Interestingly, the only portion of the crystal that is not completely ordered is a small region near the mobile loops that change in conformation on binding NO. The lack of an extended solvent region in the crystal probably contributes to the excellent diffraction of this crystal form.

In previous reports of protein structures in this resolution range, the authors have commented on the visibility of hydrogen atoms in difference maps. Although we do see some hydrogen atoms, we cannot reliably identify proton positions in this structure. In a difference electron density map calculated after anisotropic refinement of all non-hydrogen atoms, only about 40% of the aliphatic hydrogen atoms and 25% of the aromatic hydrogen atoms displayed peaks greater than 3$\sigma$ in magnitude, our criteria for visibility. The amide hydrogen atoms of the peptide chain are almost uniformly unseen.

*NP4*−*NH$_3$ at 1.15 Å Resolution.* Diffraction data for NP4−$NH_3$, pH 7.5, 100 K, were also obtained to very high resolution and refined in the same manner as NP4−NO (Table 1). The starting model was a room-temperature NP4−$NH_3$ structure of 1.5 Å resolution (*11*). In that structure, the protein was in the open conformation and electron density for loop A−B (Figure 1) was completely missing, indicating multiple conformations for the loop existed in the crystal. The present structure is very similar to the previous structure, although, with measurement at lower temperature and higher resolution, faint density for the A−B loop was visible and approximate positions could be determined. The side chains and carbonyl oxygen atoms are unseen, however, and the refined positions for these residues remain unreliable. All other atoms are visible and numerous atoms once again occupy two or three discrete conformations, including those in the heme, which, in this case, refine with 60% of the heme as "right-side-up" and 40% as "upside-down". The heme is ruffled but less so than in the NP4−NO complex (Figures 4 and 5; Table 3), and the iron lies in the plane of the pyrrole nitrogen atoms of the heme ring.

One additional difference exists between the previously reported 1.5 Å structure and the present structure. Unexpectedly, Glu 55 and Phe 107, which are well ordered and reside in the protein interior, have different conformations. At room temperature, O$\epsilon$2 of Glu 55 is hydrogen bonded, through a water molecule, to Tyr 17, and to a poorly ordered second water molecule (*11*). In the flash-frozen crystal, the waters near O$\epsilon$2 are missing, a slight collapse of the protein occurs, and Phe 107 shifts (0.6 Å) and rotates ($\Delta\chi_1 = 97°$) into the cavity previously occupied by solvent. In this arrangement, O$\epsilon$2 of Glu 55 is 3.2 Å away from Phe 107 and, although not perfectly aligned, is in an orientation that may allow a weak hydrogen bond to form with the face of the phenyl ring (*30*), assuming the group is protonated (the hydrogen atom is not visible). This same change is found in the room-temperature structure of NP4−$H_2O$ at pH 5.4 (Andersen and Montfort, unpublished observations). The Glu 55 p$K_a$ apparently increases at lower temperature, thus leading to a conformation similar to the one seen in NP4 crystallized at pH 5.6.

*NP4*−*Histamine at 1.5 Å Resolution.* Histamine is a natural ligand for NP4 and binds in the distal pocket after NO release into the victim's tissue. We have determined the structure of NP4 bound to histamine at 1.5 Å resolution, still quite high, but not of sufficient resolution for the refinement strategy used with the other structures. Anisotropic temperature factors were refined only for iron and sulfur atoms, and hydrogen atoms were not included in the calculations. All distances and angles in the model were restrained except for those of the iron coordination sphere. Only conjugate gradient refinement was performed, so errors in bond distances and angles were not calculated.

Overall, the structure is similar to that of NP1-histamine (*10*). The ligand is coordinated to iron through N$\epsilon$2 of the imidazole, refining to an Fe−N distance of 2.04 Å. The heme is ruffled to the same extent as NP4−$NH_3$ (Tables 2 and 3). The hydrogen bonds between the alkylammonium group of histamine and Asp 30 and Glu 32, and the hydrogen bond between the imidazole ring and a well-ordered water molecule, are as found for NP1-histamine (*10*). However, the carbonyl of Leu 130, which is hydrogen bonded to the histamine alkylammonium in NP1-histamine, and to Asp 30 in NP4−NO, is discretely disordered in NP4−histamine, with about half occupancy in each of the two conformations. Possibly this is due to the lower pH of this structure with respect to the NP1−histamine complex, which was determined at pH 7.5. The angle between the histamine imidazole ring and that of His 59 (32°) is similar to that in NP1−histamine (38°). Mobile loop A−B, which packs around NO in NP4−NO, is disordered in this structure.

*NP4*−*Imidazole at 1.27 Å Resolution.* We determined the structure of the NP4−imidazole complex to further characterize ligand effects on the distal pocket, since the molecule lacks the alkylamine tail of histamine, and to aid in the interpretation of spectroscopic measurements (to be reported elsewhere). The structure was determined at a temperature of 100 K and to a resolution of 1.27 Å, with strong diffraction observed even to the edge of the detector (Table 1). Consequently, we were able to refine the overall structure with anisotropic thermal parameters and refine the coordination sphere using the full-matrix of normal equations and without stereochemical restraint. Imidazole binds to NP4 in the same manner as histamine and the imidazole rings in the two structures are nearly superimposable. The positioning of the ring is restricted by van der Waals contacts with leucines 123 and 133, and through a hydrogen bond with an ordered water molecule (Figure 6). The heme in NP4−imidazole is ruffled to about the same degree as in NP4−histamine and NP4−$NH_3$ (Table 3).

Surprisingly, binding of imidazole induces closure of the NP4 distal pocket, much like that which occurs in NP4−NO. The A−B loop (Figure 1) orders into the distal pocket

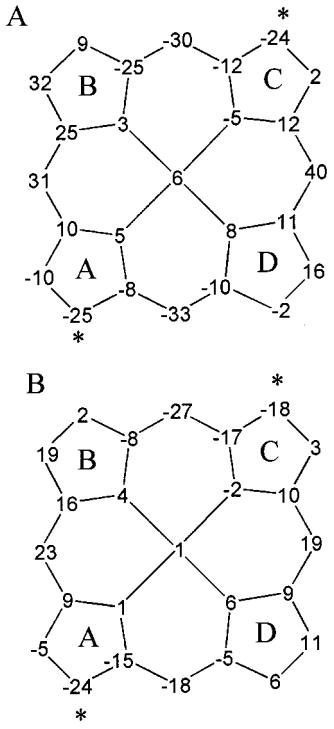


FIGURE 5: Formal core diagrams for (a) NP4−NO and (b) NP4−$NH_3$, showing deviations from the mean plane of the heme ring (units of 0.01 Å). The starred atoms are those with close contacts to the side chains of Leu 123 (C1A) and Leu 133 (C1C). Positive values indicate deviations into the distal pocket, negative values into the proximal pocket.

in a conformation nearly identical to that in NP4−NO, allowing direct contact between Val 36 and the imidazole ring (Figure 6). Differences occur between the two structures, however, in the positioning of loop G−H. In NP4−NO, this loop repositions such that Leu 130 moves well into the distal pocket and contacts the NO moiety, leaving Val 37 to pack against the outside of the leucine side chain. In contrast, Leu 130 is prevented from shifting completely into the distal pocket in NP4−imidazole through steric conflict with the imidazole ring. Instead, the G−H loop occupies two or more conformations in the NP4−imidazole structure that are part way between the open (NP4−$H_2O$, NP4−histamine) and closed (NP4−NO) conformers. Leu 130 is in contact with the imidazole ring in this arrangement and desolvation of the distal pocket appears to be complete. This result provides additional evidence in favor of the hypothesis that the hydrophobicity of NO drives the conformational change in NP4−NO (*13*), since imidazole is also a relatively hydrophobic molecule once its two nitrogens form bonds with the heme iron and a fully coordinated interior water molecule. Two conformations for the G−H loop were refined, but this model only partially explains the observed electron density.

The NP4−imidazole structure allows us to further uncouple the increase in heme ruffling from the ligand-induced protein conformational changes. As discussed in detail below, the present structures indicate that increased heme ruffling is an electronic effect due to ligand $\pi$ donation (NP4−$CN^-$, NP4−NO), and not a steric effect arising from the conformational change due to the presence of nonpolar ligands in the distal pocket (NP4−NO, NP4−imidazole).

A disordered citrate molecule found in other NP4 structures crystallized in citrate buffer at pH 5.6 is not present in this crystal. Instead, Asn 85 has taken on a different conformation, hydrogen bonding to a neighboring protein in the crystal lattice through a water molecule.

## DISCUSSION

The high resolutions of the NP4−NO, NP4−$NH_3$, and NP4−imidazole structures have allowed us to precisely determine the geometry of the ferric heme in these complexes by allowing full-matrix refinement of the iron coordination sphere without model restraints. In this way, it is possible to determine accurate bond lengths, angles, and distortions from planarity of the iron coordination sphere along with the estimated standard deviations of these values (Table 2). These results allow us to correlate the structure of the iron-containing heme in the NP4 complexes with a vast chemical and structural literature on iron porphyrin model compounds, leading to a clear view of both protein and ligand induced distortions in the heme of a *b*-heme protein.

*Bonding in Fe−NO Porphyrin Complexes.* Fe(III)NO complexes have an overall spin = 0. Using the nomenclature of Enemark and Feltham (*31*), these complexes are labeled $\{FeNO\}^6$, signifying the presence of six *d* and $\pi^*$ electrons in the FeNO bonding system (five Fe *d* electrons and the NO $\pi^*$ antibonding electron; $\sigma$ bonds are excluded). The resulting Fe−N−O bond is very strong, often described as a $\sigma$ bond and two $\pi$ bonds, and usually dominates the ligand field (*31*). To maximize the *d*-$\pi^*$ orbital overlap, these complexes must be linear in systems with undistorted octahedral symmetry, and indeed, many crystal structures of small-molecule Fe(III)NO porphyrin complexes have Fe−N−O bond angles between 175 and 180° (*32*). (Similar arguments predicated on maximizing the *d*-$\pi^*$ overlap predict that other Fe(III)-$\pi$-acceptor complexes, including $CN^-$ and $NCS^-$ will also be linear.) In contrast, Fe(II)NO complexes, denoted by $\{FeNO\}^7$, are expected to contain a bent Fe−NO group with an Fe−N−O bond angle of 120−140° (*31*, *32*). Fe(II) and Fe(III) complexes can also be distinguished by differences in the iron coordination sphere geometries. Fe(III)NO small-molecule complexes have significantly shorter Fe−N bond distances, typically around 1.66 Å, whereas in Fe(II)-NO complexes, the Fe−N bond distances are longer, around 1.72 Å (*32*). Fe(II)NO complexes also exert a strong trans influence, with the trans ligand often missing. When present, the Fe bond distance to the trans ligand is lengthened by 0.2−0.3 Å (*32*). In six-coordinate iron porphyrin model complexes, the porphyrin is generally planar within experimental error, and deviations from planarity are seen most often for porphyrins with bulky substituents attached to the ring, which require ring distortions to relieve steric crowding (reviewed in (*7*)).

*Geometry of the Fe−N−O Group in NP4 and Identification of the Iron Oxidation State.* The position of the NO ligand in the NP4−NO structure reported in this paper is unambiguous. The electron density is well defined, and the NO clearly occupies a single position (Figure 2), although there is some thermal disorder in the terminal oxygen position (Figure 3). The NP4−NO complex contains a somewhat bent Fe−NO bond angle (156°), a short Fe−N bond (1.66 Å), and a normal, not lengthened, trans Fe−His 59 bond (2.01 Å). All of these parameters, which were refined without model restraint, are consistent with those expected for an

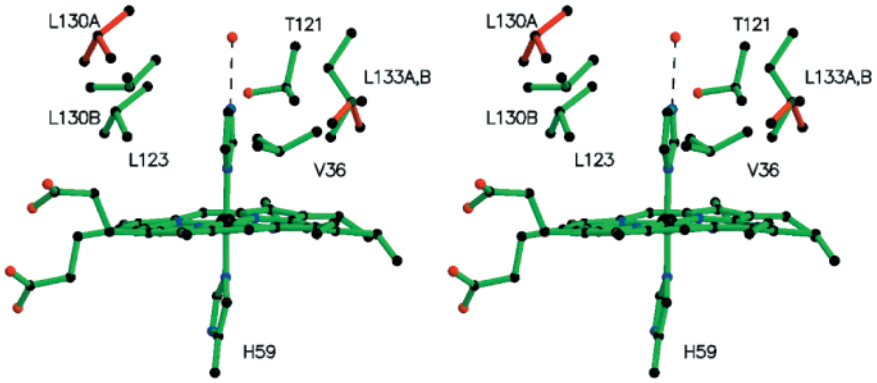


FIGURE 6: Stereoview of imidazole binding in NP4. The imidazole is oriented through heme ligation, hydrogen bonding to a structural water molecule (which forms two additional hydrogen bonds with the protein, not shown), and van der Waals contacts with Leu 123 and Leu 133. Val 36, which lies in the A−B loop, and Leu 130, which lies in the G−H loop, move into the active site in response to ligand binding, and contact the imidazole. Leu 123 and Leu 133 occupy two conformations, designated as a and b and shown in red and green. Thr 121 occupies the back of the distal pocket.

Table 4: Geometrical Parameters of Representative ML(porphyrin) Complexes

| ref code[a] (ref) | metal | M−N (Å) | angle[b] (deg) | $B_{1u}$[c] (Å) | $B_{2u}$[d] (Å) | L | compd |
|---|---|---|---|---|---|---|---|
| BEZRUT (*33*) | $Fe^{3+}$ | 2.03 | 176 | 0.158 | 0.107 | NCS | FeNCS(py)(OEP) |
| HIVGEY (*34*) | $Fe^{3+}$ | 1.67 | 169 | −0.476 | 0.141 | NO | Fe(NO)(NO2)(TpivPP)(py) |
| HIVGAU (*34*) | $Fe^{3+}$ | 1.67 | 180 | 0.115 | 0.115 | NO | Fe(NO)(NO2)(TpivPP) |
| NIPORF (*47*) | $Fe^{2+}$ | 1.74 | 144. | −0.057 | 0.079 | NO | Fe(NO)(4-Mepip)(TPP) |
| BEZRON (*33*) | $Fe^{3+}$ | 1.94 | 156 | −0.982 | 0.664 | NCS | FeNCS(py)(TPP) |

[a] Cambridge crystallographic database reference code. [b] Angle Fe-L bond and the linear L ligand. [c] Ruffling heme distortions, as defined in ref *26*. [d] Saddling heme distortions, as defined in ref *26*.

Fe(III)NO complex except the Fe−N−O bond angle, which has a value roughly halfway between the optimal values for the ferric and ferrous complexes.

Although the Fe−L bond angle is predicted to be linear in Fe(III)NO and related Fe(III) $\pi$-acceptor ligand complexes such as $CN^-$ and $NCS^-$, several complexes with bent Fe−L bonds have been observed. Two such bent complexes are particularly interesting, $FeNO(NO_2)$(tetrakis(o-pivalamidophenyl)porphyrin) and FeNCS(pyridine)(meso-tetraphenylporphyin) (*33*, *34*), because similar structures containing linear Fe−L bonds exist for both compounds. Geometrical parameters for these complexes and their analogues are given in Table 4. In both cases where significantly nonlinear Fe−L bonds exist, forcing the Fe−NO or Fe−NCS bond to be linear would have resulted in steric conflicts with porphyrin or solvent atoms. In these complexes, the porphyrin rings are also ruffled. A recently published structure of the model ferric heme nitrosyl complex (OEP)Fe−(NO)($p$-$C_6H_4F$), where OEP is octaethylporphyrinato dianion, displayed an Fe−NO bond angle of (157°) but did not have a distorted porphyrin (*35*).

In addition, the thermal ellipsoid of the terminal ligand atom is elongated in the plane containing the planar trans ligand for both model complexes with bent Fe−L bonds, suggesting that the Fe−NO bond angle is easily deformable in this plane. For our NP4−NO complex, the experimental electron density around the NO (Figure 2) and the elongated thermal ellipsoid of the oxygen atom (Figure 3) show an uncertainty in the oxygen position that would be expected if a low-energy in-plane vibrational mode existed. This bending is not stabilized through hydrogen bonding to the protein, as occurs, for example, through the distal histidine of oxymyoglobin, and so must be electronic in nature. Theoretical studies (*35*, *36*) support the hypothesis that the Fe−NO in-plane bending mode is especially low in energy. We have performed preliminary quantum mechanical calculations using the DFT method on the FeNO(heme)(histidine) complex, and the results support the idea that the Fe−NO in-plane modes are very low in energy—of about the same energy as the porphyrin distortional modes.

One as yet unexplained difference between this ultra-high-resolution structure and that reported previously (*13*) is the difference in electron density at the NO site, which was interpreted as a mixture of linear and side-on bonded NO (*13*). While we cannot yet rule out photodissociation as contributing to this discrepancy, it now appears that partial photoreduction occurred in the crystal examined with 1.54 Å X-rays but not in the crystal reported herein, which was examined with 0.98 Å X-rays. The longer wavelength X-rays are absorbed by both iron and water. Absorption by water leads to hydrated electrons that can reduce ferric heme iron even in the frozen state. For example, 1.5 Å X-rays were used to generate a reduced intermediate in crystals of P450cam (*37*). In the closed conformer of the NP4−NO complex, with a desolvated distal pocket, this reaction appears to be inhibited but not eliminated. However, in the open NP1−NO complex (*15*), or in mutant forms of NP4−NO that do not close properly (E. M. Maes and W. R. Montfort, unpublished observations), all of which have solvated distal pockets, use of 1.54 Å X-rays leads to an Fe(II)−NO complex.

*Changes in the NP4 Heme upon Ligand Binding*. Distortions in porphyrins and heme complexes are classified in terms of the low-energy vibrational modes giving rise to the distortion (*26*). The static macrocycle structure is decomposed into a linear combination of the normal modes

(vibrational distortions). The most common deformations are saddling ($B_{2u}$) (for example, deoxyhemoglobin $\beta$ chains), ruffling ($B_{1u}$) (observed in yeast ferrocytochrome *c*), and doming ($A_{2u}$) (seen in deoxyhemoglobin α chains) (*26*). These deformations can arise from steric constraints upon the heme center. For example, covalently linked hemes, as in various cytochrome *c* proteins, are often ruffled (*26*). The heme distortion affects the chemical behavior. In deoxyhemoglobin, for instance, the iron atoms bound to a heme with a doming distortion (α chain) have a higher oxygen affinity than those associated with a heme showing a saddling distortion ($\beta$ chain) (*7*). It has also been suggested that heme ruffling in tetraheme ferricytochromes $c_3$ stabilizes the Fe(III) state (*38*). In model porphyrin complexes, distortions from planarity are believed to increase the ease of oxidation of the metal center (*39*, *40*).

In the NP4−$NH_3$ structure, the bonds between the heme pyrroles and Fe are equivalent (1.99 ± 0.02 Å, Table 2), the plane defined by the pyrrole nitrogen atoms is flat, and, within experimental error, the heme iron lies in the plane of the nitrogen atoms. The pyrrole rings are rotated 4−9° about the Fe−N bonds, giving rise to a ruffled heme conformation (Figure 3; Table 3). Decomposition of the ring distortion shows that the ruffling is the largest distortion, and that some saddling is also present. This amount of ruffling is unusual for a noncovalently linked heme in a protein (*7*).

Figure 5b shows a formal core diagram for NP4−$NH_3$. The number adjacent to each atom is the distance (in units of 0.01 Å) that each atom lies either above (toward the $NH_3$) or below the mean plane of the heme ring. In NP4−$NH_3$, the macrocyclic carbon atoms with the largest deviations from the mean plane of the ligand are connected to atoms in contact with Leu 123 and Leu 133, which jut toward the heme from the distal pocket (Figure 4). Thus, heme ruffling in NP4 seems to arise from steric interactions with these side chains.

On binding NO, the heme geometry changes significantly. The rotation of the pyrrole rings becomes more pronounced (to as much as 12°, Table 3), and the iron moves out of the pyrrole nitrogen plane, into the distal pocket, by 0.06 Å. The formal core diagram for NP4−NO (Figure 5, Table 3) shows how much farther from planarity the heme ring is in NP4−NO than in NP4−$NH_3$. The heme Fe−N bond lengths do not change. Decomposition analysis shows that the heme is more distorted with ruffling in particular being increased significantly. The amount of ruffling in NP4−NO is considerably larger than in NP4−$NH_3$ and is unprecedented for a noncovalently bound heme. The close contacts that exist between heme carbons and leucine side chains in NP4−$NH_3$ persist in NP4−NO, and additional close contacts (3.6 Å) are made between Leu 130 on the mobile loop and carbons in the pyrrole D ring, which lie nearly in the mean plane of the porphyrin ring.

Is the increased ruffling of the heme in the NO complex solely due to the binding of NO, or does the loop closure contribute to the ruffling? To address these questions, we need to consider the heme conformation in the previously determined structures of NP4 complexed with $CN^-$ and water (*13*), and the NP4−histamine and NP4−imidazole structures reported herein. As shown in Table 3, on the basis of heme ruffling, NP4 complexes fall into two categories, one containing strong, $\pi$-acceptor ligands (NO, $CN^-$), and the other containing $\sigma$-donor only ($NH_3$, $H_2O$), or $\pi$-donating ligands (histamine, and imidazole). Of these, the $\pi$-acceptor ligands increase ruffling of the heme significantly and to the same extent. This increased ruffling is independent of the loop closure since loop closure was not observed in NP4−$CN^-$ (*13*), which has a more ruffled heme, and was observed in NP4−imidazole, which has no increase in heme ruffling. Thus, binding of NO or $CN^-$, both $\pi$-acceptor ligands, at the distal site appears to cause increased ruffling of the heme.

*Concurrence of Ruffled Porphyrins and Bent Fe(III)-NO, $CN^-$ Bonds.* A study of the model compounds listed in Table 4 shows that those structures containing bent Fe−L bonds also contain more ruffled porphyrins than their counterparts with linear Fe−L bonds do. These two distortions seem correlated, but as noted above, the structure of the complex (OEP)Fe−(NO)(*p*-$C_6H_4F$) shows that they are not required to occur together. Also, when a nonlinear Fe(III)-L is seen, there is often a planar trans ligand (e.g., histidine, *p*-$C_6H_4F$, or $NO_2$) oriented such that its plane bisects the planes containing the heme nitrogen atoms. The bent ligand lies in this plane and shows marked thermal anisotropy. This is also the case for our NP4−NO complex and is indicated by elongated electron density for that atom in the NP4−$CN^-$ complex, although this complex was not refined anisotropically.

Another example where a bent metal-$\pi$-acceptor ligand bond angle occurs alongside a severely ruffled porphyrin is the bis-(*tert*-butylisocyanide) complex of (OEP)Fe(III) (*41*). This complex has an EPR signal consistent with an electron configuration of $(d_{xz},d_{yz})^4(d_{xy})^1$, and the associated ruffling has been attributed mainly to an electronic effect, since the $d_{xy}$ unpaired electron does not have the proper symmetry to engage in porphyrin $\pi$ donation unless the porphyrin ring ruffles. The relative ability of porphyrin ring substituents and axial ligands to induce ruffling has been discussed (*42*, *43*). On ruffling, the nitrogen $p_z$ orbitals are twisted away from the normal to the mean heme plane and develop a component in the *xy* plane that does have the proper symmetry to overlap with the $d_{xy}$ orbital. NP4−NO is diamagnetic and therefore has no EPR signal, however planned studies on NP4 complexes with $CN^-$ and bis-(*tert*-butylisocyanide) may clarify whether this mechanism is active in NP4.

*Effect of Heme Ruffling on Stabilizing Ferric Iron.* Normally, Fe(III) nitrosyl complexes are unstable to reduction to Fe(II), but the nitrophorins must maintain a ferric nitrosyl heme to remain capable of efficient NO transport and release, as described in the introductory portion of this paper. How is this accomplished? One factor may be through the placement of negatively charged carboxylate groups near the heme (ref *15*, F. A. Walker and R. E. Berry, unpublished). A second factor may well be through heme ruffling. It is well accepted that nonplanar porphyrins are easier to oxidize and more difficult to reduce than planar porphyrins in certain model compounds (*7*, *39*, *40*). This phenomenon apparently holds true over a wide range of nonplanar distortions (saddling, ruffling), coordinated atoms (Ni, Zn, Fe, Ru, P), oxidation states, and ligand types. Although the data are sparse for systems directly corresponding to six-coordinate hemes and heme proteins, a correlation between ruffling and reduction potential has also been noted for ferricytochromes $c_3$ (*38*). In addition, theoretical work (*44*) suggests that increased heme ruffling stabilizes the Fe(III) complex relative

to the Fe(II) complex when $\pi$-acceptor ligands are present. Thus, it appears that provision of a ruffled heme may serve to maintain iron in the ferric state and prevent autoreduction of the Fe(III)NO complex in the nitrophorins. Steric contacts with protein residues appear to force the heme to be ruffled (Figure 4), thus favoring a ferric state for the iron. The closure of the mobile loops that form a hydrophobic pocket around the NO creates a tightly constrained and desolvated NO binding site that further discourages reduction, since water can assist in this reaction (*45*).

A possible mechanism for the role of heme ruffling in setting the reduction potential makes use of the $(d_{xz},d_{yz})^4(d_{xy})^1$ electron configuration described above. In this arrangement, ruffling partially fills the half-empty $d_{xy}$ orbital and interferes with reduction (*46*). Likewise, for the analogous Fe(II) heme, the extra electron fills the Fe $d_{xy}$ orbital, and the porphyrin ruffling is inhibited because that would force the overlap of completely filled $p_x$ and $d_{xy}$ orbitals. Thus, where steric interactions force a ruffled heme, such as in NP4−NO, reduction of Fe(III) is disfavored.

Another possible contribution to the stabilization of the Fe(III) complex in NP4−NO is the need to lengthen or dissociate the bond to His 59 when the Fe(II) complex forms. Once the Fe(III)NO bond is formed and the mobile loop packs against the NO, the heme cavity is quite tightly packed and lengthening of the Fe−His 59 bond may be disfavored.

*Protonation State of Glu 55 Apparently Changes When the Crystal Is Frozen.* We have previously suggested that Glu 55, which lies in the protein interior, may be one of the residues involved in pH signaling since its hydration differs at low and high pH in room-temperature structures (ref *11* and J. F. Andersen and W. R. Montfort, unpublished results). In the frozen crystal of NP4−$NH_3$, the environment around Glu 55 is identical with that seen in the pH 5.6 structure at room temperature, even though the crystal was grown at pH 7.5. Thus, even though freezing of the crystal was rapid, it appears that protonation of Glu 55 and solvent expulsion has occurred. This may or may not be of functional importance for NP4, however, as crystallographers move toward collecting data solely from frozen crystals to reduce crystal decay, it is important to keep in mind the possibility of such temperature-dependent structural changes occurring when crystals are frozen.

## ACKNOWLEDGMENT

We thank Dr. Ken Knudsen for help with data measurement at the ESRF, the Biozentrum structure group for help with reduction of these data, Dr. Klaus Schroer for help with data measurement at the NSLS, Dr. John Enemark for many helpful discussions, and Dr. Robert Scheidt for sharing data before publication. Sandia is a multiprogram laboratory operated by Sandia Corporation, a Lockheed-Martin company, for the United States Department of Energy under Contract DE-AC04-94AL85000.

## REFERENCES

1. Stuehr, D. J. (1999) *Biochim. Biophys. Acta 1411*, 217−230.
2. Denninger, J. W., and Marletta, M. A. (1999) *Biochim. Biophys. Acta 1411*, 334−350.
3. Koesling, D. (1999) *Methods 19*, 485−493.
4. Ludwig, M. L., and Marletta, M. A. (1999) *Struct. Folding Des. 7*, R73−R79.
5. Ribeiro, J. M. C., Hazzard, J. M. H., Nussenzveig, R. H., Champagne, D. E., and Walker, F. A. (1993) *Science 260*, 539−541.
6. Valenzuela, J. G., Walker, F. A., and Ribeiro, J. M. C. (1995) *J. Exp. Biol. 198*, 1519−1526.
7. Shelnutt, J. A., Song, X.-Z., Ma, J.-G., Jia, S.-L., Jentzen, W., and Medforth, C. J. (1998) *Chem. Soc. Rev. 27*, 31−41.
8. Montfort, W. R., Weichsel, A., and Andersen, J. F. (2000) *Biochim. Biophys. Acta 1482*, 110−118.
9. Walker, F. A., and Montfort, W. R. (2000) in *Advances in Inorganic Chemistry* (Sykes, A. G., Ed., and Mauk, G., Eds.) Vol. 51, pp 295−358, Academic Press, San Diego.
10. Weichsel, A., Andersen, J. F., Champagne, D. E., Walker, F. A., and Montfort, W. R. (1998) *Nat. Struct. Biol. 5*, 304−309.
11. Andersen, J. F., Weichsel, A., Balfour, C. A., Champagne, D. E., and Montfort, W. R. (1998) *Structure 6*, 1315−1327.
12. Andersen, J. F., and Montfort, W. R. (2000) *J. Biol. Chem. 275*, 30496−30503.
13. Weichsel, A., Andersen, J. F., Roberts, S. A., and Montfort, W. R. (2000) *Nat. Struct. Biol. 7*, 551−554.
14. Andersen, J. F., Ding, X. D., Balfour, C., Shokhireva, T. K., Champagne, D. E., Walker, F. A., and Montfort, W. R. (2000) *Biochemistry 39*, 10118−10131.
15. Ding, X. D., Weichsel, A., Andersen, J. F., Shokhireva, T. K., Balfour, C., Pierik, A. J., Averill, B. A., Montfort, W. R., and Walker, F. A. (1999) *J. Am. Chem. Soc. 121*, 128−138.
16. Andersen, J. F., Champagne, D. E., Weichsel, A., Ribeiro, J. M. C., Balfour, C. A., Dress, V., and Montfort, W. R. (1997) *Biochemistry 36*, 4423−4428.
17. Otwinowski, Z., and Minor, W. (1997) *Methods Enzymol. 276*, 307−326.
18. Collaborative Computational Project Number 4. (1994) *Acta Crystallogr., Sect. D 50*, 760−763.
19. Kabsch, W. (1988) *J. Appl. Crystallogr. 21*, 916−934.
20. Pflugrath, J. W. (1999) *Acta Crystallogr., Sect. D 55*, 1718−1725.
21. Jones, T. A., Zou, J. Y., Cowan, S. W., and Kjelgard, M. (1991) *Acta Crystallogr., Sect. A 47*, 110−119.
22. Sheldrick, G. M., and Schneider, T. R. (1997) *Methods Enzymol. 277*, 319−343.
23. Kraulis, P. J. (1991) *J. Appl. Crystallogr. 24*, 946−950.
24. Esnouf, R. M. (1997) *J. Mol. Graph. Model 15*, 132−134, 112−113.
25. Merritt, E. A., and Murphy, M. E. P. (1994) *Acta Crystallogr., Sect. D 50*, 869−873.
26. Jentzen, W., Song, X.-Z., and Shelnutt, J. A. (1997) *J. Phys. Chem. B. 101*, 1684−1699.
27. McLachlan, S. J., La Mar, G. N., Burns, P. D., Smith, K. M., and Langry, K. C. (1986) *Biochim. Biophys. Acta 874*, 274−284.
28. Keller, R. M., and Wüthrich, K. (1980) *Biochim. Biophys. Acta 621*, 204−217.
29. Walker, F. A., Emrick, D., Rivera, J. E., Hanquet, B. J., and Buttlaire, D. H. (1988) *J. Am. Chem. Soc. 110*, 6234−6240.
30. Steiner, T., Schreurs, A. M. M., Kanters, J. A., and Kroon, J. (1998) *Acta Crystallogr., Sect. D 54*, 25−31.
31. Enemark, J. H., and Feltham, R. D. (1974) *Coord. Chem. Rev. 13*, 339−406.
32. Scheidt, W. R., and Ellison, M. K. (1999) *Acc. Chem. Res. 32*, 350−359.
33. Scheidt, W. R., Lee, Y. J., Geiger, D. K., Taylor, K., and Hatano, K. (1982) *J. Am. Chem. Soc. 104*, 3367−3374.
34. Ellison, M. K., Schulz, C. E., and Scheidt, W. R. (1999) *Inorg. Chem. 38*, 100−108.
35. Richter-Addo, G. B., Wheeler, R. A., Hixson, C. A., Chen, L., Khan, M. A., Ellison, M. K., Schulz, C. E., and Scheidt, W. R. (2001) *J. Am. Chem. Soc. 123*, 6314−6326.
36. Vangberg, T., Bocian, D. F., and Ghosh, A. (1997) *J. Biol. Inorg. Chem. 2*, 526−530.
37. Schlichting, I., Berendzen, J., Chu, K., Stock, A. M., Maves, S. A., Benson, D. E., Sweet, R. M., Ringe, D., Petsko, G. A., and Sligar, S. G. (2000) *Science 287*, 1615−1622.

38. Ma, J. G., Zhang, J., Franco, R., Jia, S. L., Moura, I., Moura, J. J., Kroneck, P. M., and Shelnutt, J. A. (1998) *Biochemistry 37*, 12431−12442.
39. Senge, M. O. (2000) in *The Porphyrin Handbook* (Kadish, K. M., Smith, K. M., and Guilard, R., Eds.) Vol. 1, pp 240−347, Academic Press, San Diego.
40. Kadish, K. M., Van Camelbecke, E., and Royal, G. (2000) in *The Porphyrin Handbook* (Kadish, K. M., Smith, K. M., and Guilard, R., Eds.) Vol. 8, pp 3−125, Academic Press, San Diego.
41. Walker, F. A., Nasri, H., Turowska-Tyrk, I., Mohanroa, K., Watson, C. T., Shokhirev, N. V., Debrunner, P. G., and Scheidt, W. R. (1996) *J. Am. Chem. Soc. 118*, 12109−12118.
42. Nakamura, M., Ikeue, T., Ikezaki, A., Ohgo, Y., and Fujii, H. (1999) *Inorg. Chem. 38*, 3857−3862.
43. Ikeue, T., Ohgo, Y., Saitoh, T., Nakamura, M., Fujii, H., and Yokoyama, M. (2000) *J. Am. Chem. Soc. 122*, 4068−4076.
44. Ghosh, A. (2000) in *The Porphyrin Handbook* (Kadish, K. M., Smith, K. M., and Guilard, R., Eds.), Vol. 7, pp 1−38, Academic Press, San Diego.
45. Hoshino, M., Maeda, M., Konishi, R., Seki, H., and Ford, P. C. (1996) *J. Am. Chem. Soc. 118*, 5702−5707.
46. Walker, F. A. (1999) *Coord. Chem. Rev. 185*−*186*, 471−534.
47. Scheidt, W. R., Brinegar, A. C., Ferro, E. B., and Kirner, J. F. (1977) *J. Am. Chem. Soc. 99*, 7315−7322.

BI0109257